Available online at www.sciencedirect.com

ScienceDirect

Procedia Structural Integrity 19 (2019) 548–555

Structural Integrity Procedia

www.elsevier.com/locate/procedia

Fatigue Design 2019

Numerical simulation of cyclic plasticity in mechanical components under low cycle fatigue loading: accelerated material models

J. Srnec Novak[a,]*, F. De Bona[a] and D. Benasciutti[b]

[a]*Politechnic Department of Engineering and Architecture (DPIA), University of Udine, via delle Scienze 208, Udine 33100, Italy*
[b]*Department of Engineering, University of Ferrara, via Saragat 1, Ferrara 44122, Italy*

Abstract

Numerical simulations of components subjected to low-cycle fatigue loading require an accurate modeling of the material cyclic plasticity behavior until complete stabilization. In some circumstances, especially in case of small plastic strains, it may happen that the material model needs a huge number of cycles to reach complete stabilization, which results into an unfeasible simulation time. An acceleration technique, based on a fictitious increase of the parameter that controls the speed of stabilization in the combined (kinematic and isotropic) model, may be used. To check the efficiency and the correctness of the acceleration technique, the case of a welded cruciform joint under low cycle fatigue, taken from the literature, is here considered. The joint can be analyzed with a two-dimensional finite element model, which permits a relatively fast simulation to be completed until stabilization even with a combined kinematic-isotropic plasticity model (reference case). A comparison of this reference case with accelerated models is performed. Results in term of equivalent total strain range show that the acceleration procedure does not alter the welded joint cyclic behavior at stabilization, whereas it drastically reduces the computational time.

Peer-review under responsibility of the Fatigue Design 2019 Organizers.

Keywords: accelerated techniques, cruciform, cyclic plasticity, FEM, material models;

* Corresponding author. Tel.: +39-(0)432-558297; fax: +39-(0)432-558251.
E-mail address: jelena.srnec@uniud.it

2452-3216
Peer-review under responsibility of the Fatigue Design 2019 Organizers.
10.1016/j.prostr.2019.12.059

1. Introduction

Durability assessment of mechanical components undergoing low cycle fatigue often requires an elasto-plastic finite element (FE) analysis. It is worth noting that, to perform a fatigue life assessment, stabilization of the material cyclic behavior has to be achieved (Manson (1966)). Hence, in the case of FE models with a high number of elements, the computational time could increase so much to become not acceptable. A possible relief to speed up simulation is that of making use of acceleration techniques. In Srnec Novak et al. (2018), the cyclic plasticity behavior of a copper alloy was modelled by using a combined kinematic (Amstrong-Frederick) and isotropic (Voice) model, whose speed of stabilization was increased "fictitiously" to achieve a significant reduction of the number of cycles required to reach stabilization. The aforementioned method was tested in the case of a copper mold for steelmaking plant subjected to cyclic thermal loads. Due to the axi-symmetry of the component, a plane model could be used thus permitting the correctness of the acceleration techniques to be verified by comparison with the reference "not-accelerated" case. The aim of this work is to test the possibility to apply the proposed approach to other material and loading conditions. For example, Saiprasertkit et al. (2012) recently assessed the low cycle fatigue life curve of a cruciform welded joint by a notch strain approach, in which a "local" strain (maximum equivalent total strain range) is evaluated by means of an elasto-plastic FE analysis according to the effective notch concept. The proposed case study seems particularly suitable for investigating the feasibility of an acceleration technique. In fact, firstly the weld geometry can be described with a plane model, thus permitting a relatively fast simulation. Secondly, the example adopts a material cyclic plasticity model similar to that employed in Srnec Novak et al. (2018), which allows one to easily follows the same procedure by which the "fictitious" speed of stabilization is determined.

Nomenclature

b	speed of stabilization	γ	non-linear recovery parameter
b_a	accelerated speed of stabilization	$\Delta\gamma_p$	shear plastic strain range
C	hardening modulus	$\Delta\varepsilon_{eff}$	effective notch strain range
$d\varepsilon_{pl}$	plastic strain increment	$\Delta\varepsilon_{eq,notch}$	equivalent total strain range in notch
$d\varepsilon_{pl,acc}$	accumulated plastic strain increment	$\Delta\varepsilon_{pl}$	plastic strain range
e	relative difference	$\Delta\varepsilon_{pl,eq}$	equivalent plastic strain range
E	Young's modulus	$\Delta\varepsilon_{x,notch}$	x component of plastic strain range (notch)
N	number of cycles	$\Delta\varepsilon_{x,ref}$	x component of plastic strain range (ref. position)
N_{stab}	number of cycles to stabilization	$\Delta\sigma$	stress range
r	radius	$\Delta\sigma_{eq}$	equivalent stress range
R	drag stress	$\Delta\tau$	shear stress range
R_∞	saturation value	$\varepsilon_{pl,acc}$	accumulated plastic strain
$\boldsymbol{S}$	deviatoric stress tensor	$\varepsilon_{vM,pl}$	von Mises plastic strain
u	imposed displacement	σ_0	initial yield stress
$\boldsymbol{X}$	deviatoric back stress tensor	σ_{vM}	von Mises stress
x,y,z	Cartesian axes		

2. Theoretical background of cyclic plasticity models

The yield surface can be represented considering combined kinematic and isotropic model as, Lemaitre (1990):

$$\sqrt{\frac{3}{2}(\boldsymbol{S}-\boldsymbol{X}):(\boldsymbol{S}-\boldsymbol{X})} - R - \sigma_0 = 0 \tag{1}$$

where $\boldsymbol{S}$ and $\boldsymbol{X}$ is the deviatoric stress tensor and the deviatoric back-stress tensor, respectively, R is the drag stress and σ_0 is the initial yield stress. Kinematic part is controlled by $\boldsymbol{X}$ (translation of the yield surface), while isotropic part is managed by R (expansion of the yield surface).

The nonlinear kinematic (Chaboche model) assumes that the increment of the back stress dX is expressed as a function of the plastic strain increment d$\boldsymbol{\varepsilon}_{\mathrm{pl}}$ and accumulated plastic strain increment d$\varepsilon_{\mathrm{pl,acc}}$:

$$\boldsymbol{X} = \sum_{\mathrm{i}=1}^{n} \boldsymbol{X}_{\mathrm{i}} \quad ; \quad \mathrm{d}\boldsymbol{X}_{\mathrm{i}} = \frac{2}{3} C_{\mathrm{i}} \mathrm{d}\boldsymbol{\varepsilon}_{\mathrm{pl}} - \gamma_{\mathrm{i}} \boldsymbol{X}_{\mathrm{i}} \mathrm{d}\varepsilon_{\mathrm{pl,acc}} \tag{2}$$

where C is the hardening modulus and γ is the recovery parameter controlling the decay of C as plastic strain accumulates. Eq. (2) for i=1 (i.e. with two pair of C_1 and γ_1) yields the Armstrong-Frederick model.

Cyclic hardening/softening phenomenon is controlled by the isotropic part through the incremental relationship $\mathrm{d}R=b(R_\infty - R)\mathrm{d}\varepsilon_{\mathrm{pl,acc}}$, in which R_∞ is the saturated stress and b is the stabilization speed for hardening ($R_\infty>0$) or softening ($R_\infty<0$). In the uniaxial case, integrating the previous expression gives:

$$R = R_\infty \left[1 - \exp\left(-b\varepsilon_{\mathrm{pl,acc}}\right)\right] \tag{3}$$

The material stabilizes when R reaches R_∞, which, according to Chaboche (2018) occurs approximately when the exponent in Eq. (3) is $b\varepsilon_{\mathrm{pl,acc}}\approx 5$. Cyclic hardening/softening evolution is governed by the speed of stabilization b and the accumulated plastic strain $\varepsilon_{\mathrm{pl,acc}}$ which in case of strain-controlled loading after N cycles is equal to $\varepsilon_{\mathrm{pl,acc}}\approx 2N\Delta\varepsilon_{\mathrm{pl}}$ (where $\Delta\varepsilon_{\mathrm{pl}}$ is the plastic strain range). Based on this assumptions, the stabilized condition is obtained when:

$$2bN_{\mathrm{stab}}\Delta\varepsilon_{\mathrm{pl}} \approx 5 \tag{4}$$

where N_{stab} is the number of cycles to stabilization, which may become really large in those situations when b and $\Delta\varepsilon_{\mathrm{pl}}$ are relatively small.

Some accelerated techniques thus have been proposed in the literature to overcome large-scale FE simulations. In presence of creep and thermal fatigue, some authors like Amiable et al. (2006) and Arya et al. (1990) suggest to simulate only a limited number of cycles. Although not well defined, this procedure could be justified by considering that presence of visco-elasticity generally tends to reduce the time to stabilization. Instead, Kontermann et al. (2014) developed and proposed an extrapolation technique to speed up the simulation in case that the creep rupture constitutes the damage criterion in design. In situations when creep is absent, some authors as Li et al. (2006) and Campagnolo et al. (2016) suggest that the kinematic model with stabilized material properties has to be adopted from the beginning of simulation, at the same time neglecting the initial state of material. On the other hand, Sviliopoulos et al. (2012) proposed a direct method (Residual Stress Decomposition Method - RSDM) which is able to find, right from the start of the calculation, the characteristic asymptotic steady state behavior of an elasto-perfectly plastic structure under cyclic loading.

3. Case study: cruciform welded joint under low cycle fatigue loadings

The cruciform welded joint in Fig. 1(a), described in Saiprasertkit et al. (2012), is here considered as a case study. That work investigated welded specimens with different degrees of incomplete penetration (from 25% to 100%) and various strength mismatching between base and weld metal. Specimens were subjected to low cycle fatigue tests at four strain range values (with root and toe-root cracks) with the aim of estimating the strain-life curves. Tests results plotted in a (strain range/cycles) diagram showed, however, a certain scatter attributed to the different combinations of incomplete penetration and strength mismatch, which affected the local elasto-plastic strain behaviour in crack initiation point (root and toe) of tested specimens. The study thus proposed to correlate the fatigue strength to a local strain parameter (equivalent strain range). For this purpose, the local strain value was evaluated according to an elasto-plastic finite element modelling according to the effective notch concept, see Hobbacher (2016).

The analysis described in the following is focused on a particular weld geometry (categorized as P100-U25), which is constituted by 16 mm plates in JIS SBHS500 structural steel, and it is characterized by 100% incomplete penetration (i.e. the joint has fillet welds) and 25% strength under-matching. The weld is subjected to a constant amplitude displacement with range 0.11 mm, see Fig. 1(c).

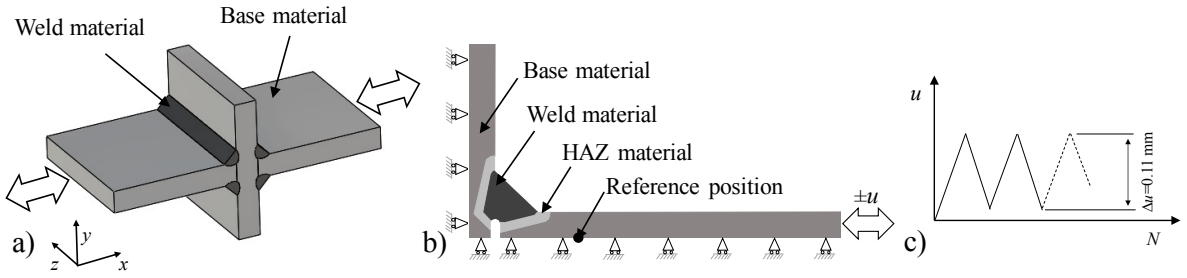

Fig. 1. (a) Cruciform welded joint; (b) model and boundary conditions; (c) loading condition.

3.1. Numerical model

A finite element model is built based on the geometry of P100-U25 specimen. Thanks to the double symmetry, only one-quarter model is considered, see Fig. 1(b). Following Saiprasertkit et al. (2012), three distinct zones are identified to distinguish the mechanical properties of base metal, heat affected zone (HAZ) and weld metal. In order to apply the effective notch strain concept, a fictitious U-shaped notch with radius r=1 mm is introduced in the weld geometry, following the recommendations given in Hobbacher (2016) and Fricke (2013).

The geometry is meshed by quadrilateral 8-node and triangular 6-node finite elements (for a total of 2820 elements and 8693 nodes) in plain strain condition. Fig. 2 shows a detail of the mesh in the welded region. While a relatively coarse mesh is established far away from the weld bead, a locally refined mesh is used close to the fictitious notch. Mesh is made to vary gradually to avoid element distortion. Close to the U-notch and the weld toe, the mesh has 0.1×0.1mm elements, i.e. far below the recommended size of r/4. A convergence analysis is also performed to confirm that a finer mesh would only give a 0.4% difference in results.

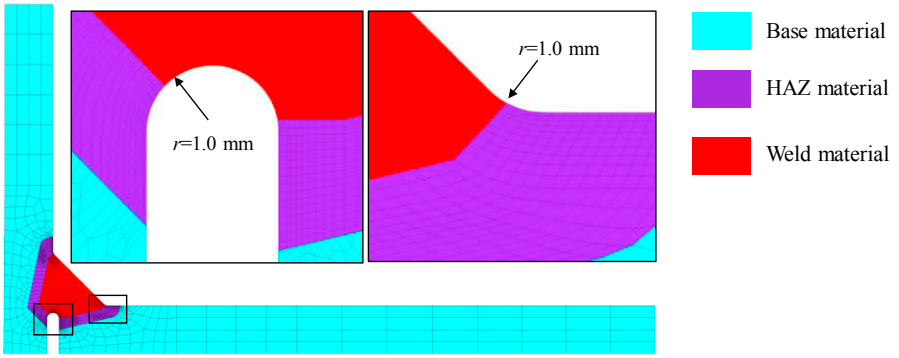

Fig. 2. Finite element mesh with detailed view of weld toe and root.

The simulation replicates the experimental tests performed by Saiprasertkit et al. (2012), in which the displacement u was applied at the far end of the plate. In the numerical analysis, the maximum value of u is determined so that the local displacement in reference position (see Fig. 1(b)) matches exactly the value measured, in the same location, by a transducer during the tests. The minimum value of u at the end of unloading is determined by the same procedure.

A combined nonlinear kinematic and isotropic material model ("reference model") is used for simulating the cyclic behavior of all three materials (base metal, weld metal and HAZ) in the welded joint. Material parameters are summarized in Table 1. In the under-matched weld under study, the weld metal has a lower strength than base metal. By contrast, the HAZ has an initial yields stress that is 20% higher than base metal, whereas it has same kinematic and isotropic parameters as base metal.

Table 1. Material parameters taken from Hanji et al. (2011) and Saiprasertkit et al. (2012).

Material	E (GPa)	σ_0 (MPa)	C (MPa)	γ	R_∞ (MPa)	b
Base metal SBHS500-2	200	452	190	36	143	4
HAZ	200	542	190	36	143	4
Weld metal	200	328	215	92	113	1

An elasto-plastic FE analysis is performed according to the load history shown in Fig. 1(c). The calculation is carried out up to material stabilization is reached. As proposed in Saiprasertkit et al. (2012), the critical point is that experiencing the maximum value of the equivalent total strain range $\Delta\varepsilon_{\text{eq,notch}}$, which is used as the effective notch strain range $\Delta\varepsilon_{\text{eff}}$. The equivalent total strain range is the summation of the elastic and plastic components:

$$\Delta\varepsilon_{\text{eff}} = \Delta\varepsilon_{\text{eq, notch}} = \frac{\Delta\sigma_{\text{eq}}}{E} + \Delta\varepsilon_{\text{pl,eq}} \tag{5}$$

$$\Delta\sigma_{\text{eq}} = \sqrt{\frac{1}{2}\left[\left(\Delta\sigma_{\text{x}} - \Delta\sigma_{\text{y}}\right)^2 + \left(\Delta\sigma_{\text{y}} - \Delta\sigma_{\text{z}}\right)^2 + \left(\Delta\sigma_{\text{z}} - \Delta\sigma_{\text{x}}\right)^2 + 6\left(\Delta\tau_{\text{xy}}^2 + \Delta\tau_{\text{yz}}^2 + \Delta\tau_{\text{zx}}^2\right)\right]} \tag{6}$$

$$\Delta\varepsilon_{\text{pl,eq}} = \frac{1}{3}\sqrt{2\left[\left(\Delta\varepsilon_{\text{p,x}} - \Delta\varepsilon_{\text{p,y}}\right)^2 + \left(\Delta\varepsilon_{\text{p,y}} - \Delta\varepsilon_{\text{p,z}}\right)^2 + \left(\Delta\varepsilon_{\text{p,z}} - \Delta\varepsilon_{\text{p,x}}\right)^2 + \frac{3}{2}\left(\Delta\gamma_{\text{p,xy}}^2 + \Delta\gamma_{\text{p,yz}}^2 + \Delta\gamma_{\text{p,zx}}^2\right)\right]} \tag{7}$$

where $\Delta\sigma$ is the normal stress range, $\Delta\tau$ is the shear stress range, $\Delta\varepsilon_{\text{p}}$ is the plastic strain range, $\Delta\gamma_{\text{p}}$ is the shear plastic strain range, $\Delta\sigma_{\text{eq}}$ is the equivalent stress range, $\Delta\varepsilon_{\text{pl,eq}}$ is the equivalent plastic strain range.

3.2. Reference case: cyclic behavior up to stabilization

The results of the reference case (i.e. not-accelerated material model) are considered first. Simulation shows that the maximum stress is always located at the weld toe and increases over cycles, see Fig. 3. At the first loading, plasticization occurs only in a localized area between the weld root and toe. As the number of applied cycles increases, a significant stress redistribution takes place while the plasticization area enlarges (see Fig. 4), similarly to the study presented in Hanji et al. (2011).

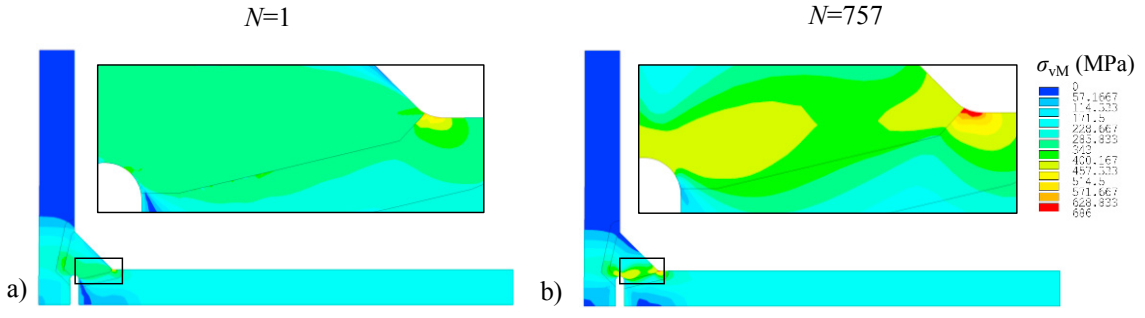

Fig. 3. Von Mises stress distribution: (a) first cycle; (b) stabilized cycle.

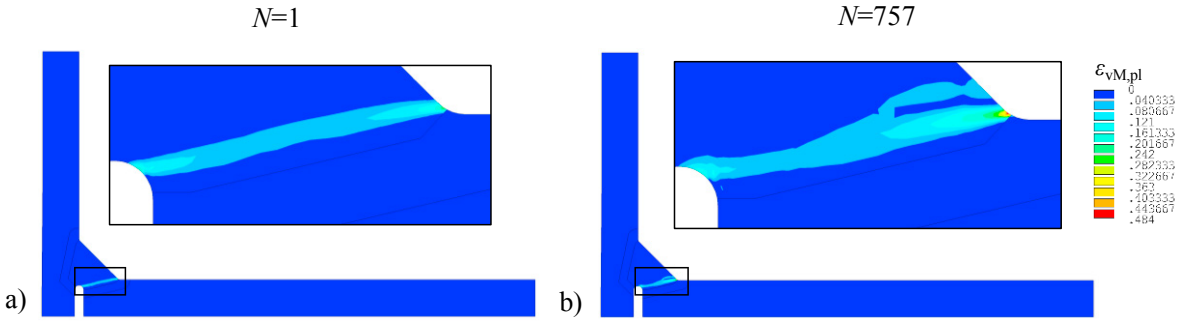

Fig. 4. Von Mises plastic strain: (a) first cycle; (b) stabilized cycle.

As shown in Fig. 5(a), the stress increases (i.e. material exhibit cyclic hardening) up to 100 cycle when saturation is reached, whereas strains progressively decrease over cycles, see Fig. 5(b). Hence, the "stabilization criterion" (used to identify the number of cycles at which material stabilizes) cannot be defined in terms of stress, but of strains. Here it is proposed to compute the relative difference of the equivalent strain range between two subsequent cycles:

$$\Delta e_{\mathrm{eq,notch}} = \left(\frac{\left| \Delta\varepsilon_{\mathrm{eq,notch}}(i) - \Delta\varepsilon_{\mathrm{eq,notch}}(i+1) \right|}{\Delta\varepsilon_{\mathrm{eq,notch}}(i)} \right) \times 100 \tag{8}$$

and to compare it with a given threshold (0.002). According to the adopted criterion, $\Delta e_{\mathrm{eq,notch}} \leq 0.002$, stabilization is reached after 757 cycles. If, instead, the procedure described in Srnec Novak et al. (2018) is followed, in which the cycles to stabilization are estimated through Eq. (4) by using the plastic strain range calculated after five cycles ($\Delta\varepsilon_{\mathrm{pl,5}}$), a much lower number would result (≈260 cycles). This significant difference can be probably explained by taking into account the cyclic hardening that causes gradually decreasing of the plastic strain range over cycles and, therefore, an underestimated value of N_{stab} is obtained when $\Delta\varepsilon_{\mathrm{pl,5}}$ is considered.

After stabilization, a maximum equivalent strain range $\Delta\varepsilon_{\mathrm{eq,notch}}=0.0199$ is recorded. This value is in good agreement (1.53% relative difference) with that obtained by Saiprasertkit et al. (2012), see also Table 2.

Fig. 5(b) confirms that the numerical model well describes the aforementioned experimental procedure. In fact, in that case the experimental set-up guarantees a constant imposed strain in the reference position, which is actually observed also in the present simulation. On the other hand, the previously mentioned stress redistribution makes the strain range not constant in the area close to the fictitious notch.

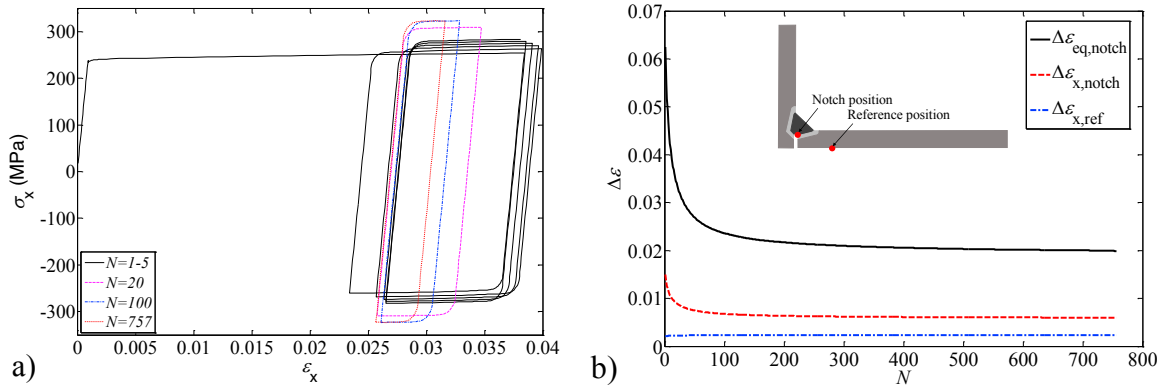

Fig. 5. (a) Combined model: stress-strain cycles in *x*-direction; (b) strain range versus number of cycles.

3.3. Accelerated material models

The previous results show that the reference material model needs a hundreds of cycles to reach stabilization, which results in a rather high computational time (more than 6 hours). If the same material model were used in the analysis of a welded joint that needs a 3D finite element model, the computational time would clearly exceed any practical limit. In the attempt to speed-up the simulation, this work tries to apply the procedure proposed in Srnec Novak et al. (2018), in which the basic idea is that of increasing the speed of stabilization b.

Results from the reference case (combined nonlinear kinematic and nonlinear isotropic material model with b as per experiments) are thus compared with those achieved by a set of accelerated models with 9 increased values of b_a: 5b, 10b, 20b, 50b, 100b, 150b, 1500b, 2500b and 5000b (note that these values cover a wider range with respect to that proposed by Chaboche (1986)). As shown in Fig. 6, for increasing values of b_a stabilization occurs faster. Already for a value of b_a=5b the number of cycles to stabilization is more than halved. For b_a=20b, it is N_{stab}=122, while for even higher values of b_a no significant decrease of N_{stab} is obtained. On the other hand, the convergence is always achieved even if a slight numerical instability occurs for b_a=100b or even higher.

As expected from Eq. (4), the correlation between the speed of stabilization b and the number of cycles to stabilization N_{stab} is linear in a log-log diagram. However, results show (see Fig. 6(b)) that such a linear relationship is only fulfilled up to b_a=20b (≈1 hour). At higher values of b_a the number of cycles to stabilization remains constant. This behavior was not observed in Srnec Novak et al. (2018) in the case of a copper alloy. On the other hand, in that study in which the material exhibited a cyclic softening behavior and underwent a fully reversed strain, an upper bound value of b_a was identified, above which the numerical analysis did not converge. On the contrary, in the study presented here (cyclic hardening, not fully reversed cycles) the numerical convergence is always achieved, even for very high value of b_a.

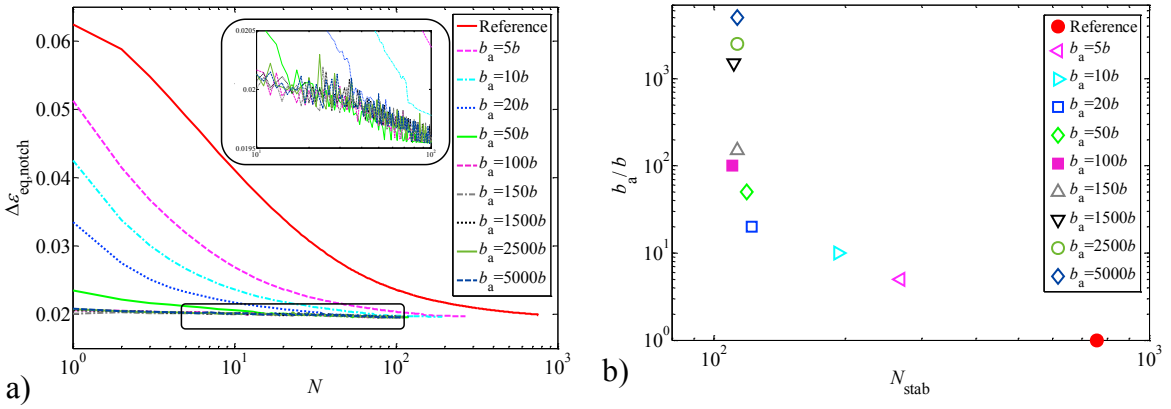

Fig. 6. (a) Equivalent strain range versus number of cycles to stabilization; (b) Correlation between speed of stabilization and number of cycles to stabilization.

Table 2 reports the difference obtained by comparing the reference case (b) with the accelerated models (b_a). All cases give almost the same value of equivalent strain range with small difference.

Table 2. Number of cycles to stabilization and $\Delta\varepsilon_{eq,notch}$.

	P100-U25[a]	Reference model	Accelerated models								
			5b	10b	20b	50b	100b	150b	1500b	2500b	5000b
N_{stab}		757	268	193	122	119	110	113	111	113	113
$\Delta\varepsilon_{eq,notch}$	0.0196	0.0199	0.0197	0.0196	0.0196	0.0195	0.0195	0.0195	0.0195	0.0195	0.0195
e (%)		1.53[b]	-1.01[c]	-1.51[c]	-1.51[c]	-2.01[c]	-2.01[c]	-2.01[c]	-2.01[c]	-2.01[c]	-2.01[c]

[a] Saiprasertkit et al. (2012), [b] relative difference calculated with respect to P100-U25, [c] relative difference calculated with respect to the reference model

4. Conclusions

A fictitious increase of the parameter b governing the speed of stabilization seems a promising strategy to speed-up an elasto-plastic finite element simulation, when a too high computational time is required to reach stabilization. If applied to the case of a load-carrying cruciform welded joint already studied in the literature, the proposed approach permits the computational time to be drastically reduced with a negligible difference (< 2%) from the results of a reference case that uses the actual material properties. The elasto-plastic material behavior of the three materials in the welded joint (base metal, weld metal and HAZ) is described with a combined nonlinear kinematic and isotropic model. Owing to the fact that materials exhibit cyclic hardening and the applied displacement is not fully reversed, a preliminary estimation of the number of cycles to reach stabilization seems uncertain and thus a preliminary evaluation of the computational time seems not possible. On the other hand, convergence to the correct value is always reached, also for a huge value of b_a, hence it is possible to foresee a simple guideline to perform a correct analysis when the FE model dimension makes the simulation of the not-accelerated case impossible. Some simulation (at least 2 or 3) must be planned, starting with a high speed of stabilization (b_a/b>1000) and then adopting smaller values of b_a (it would be desirable, compatibly with the computational time, to span a range of b_a covering 1 or 2 orders of magnitude). If convergence always occurs and the effective notch strain $\Delta\varepsilon_{eff}$ remains almost constant, the correctness of the simulation should be guaranteed and the obtained local strain parameter can be adopted. If, unlike what is observed in this work, convergence is not reached or a significant difference in the obtained notch strain values is reported, a higher computational effort would be required, as a value of speed of stabilization under which results remain almost constant, has to be assessed.

References

Amiable, S., Chapuliot, S., Constantinescu, A., Fissolo, A., 2006, A Computational Lifetime Prediction of a Thermal Shock Experiment. Part I. Thermomechanical modelling and Lifetime Prediction, Fatigue & Fracture of Engineering Materials & Structures, 29, 209–217.

Arya, V. K., Melis, M. E., Halford, G. R., 1990, Finite Element Elastic-Plastic-Creep and Cyclic Life Analysis of a Cowl Lip (NASA Technical memorandum 102342).

Campagnolo, A., Berto, F., Marangon, C., 2016, Cyclic Plasticity in Three-dimensional notch components under In-phase Multiaxial Loading at R=-1, Theoretical and Applied Fracture Mechanics, 81, 76-88.

Chaboche, J. L., Cailletaud, G., 1986, On the Calculation of Structures in Cyclic Plasticity or Viscoplasticity, 23, 23-31.

Chaboche, J. L., 2008, A Review of some Plasticity and Viscoplasticity Theories, International Journal of Plasticity, 24, 16-42-1693.

Lemaitre, J., Chaboche, J.L., 1990, Mechanics of solid materials, Cambridge University Press, Cambridge.

Li, B., Reis, M., de Freitas, M., 2006, Simulation of Cyclic Stress/strain Evaluations for Multiaxial Fatigue Life Prediction, International Journal of Fatigue, 28, 451-458.

Fricke, W., 2013, IIW Guidelines for the Assessment of Weld Root Fatigue, Research Paper, Weld World 57, 753-791.

Hanji, T., Saiprasertkit, K., Miki, C., 2011, Low- and High-cycle Fatigue Behavior of Load-carrying Cruciform Joints with Incomplete Penetration and Strength Under-match, International Journal of Steel Structures 11, 409-425.

Hobbacher, A.F., 2016, Collection Recommendations for Fatigue Design of Welded Joints and Components, 2nd Ed, (IIW doc. IIW-2259-15, ex XIII-2460-13/XV-1440-13. This document is a revision of XIII-2151r4-07/XV-1254r4-07, Springer.

Konterman, C., Scholz, A., Oechsner, M., 2014, A Method to Reduce Calculation Time for FE Simulations using constitutive material models, Materials at High Temperatrue, 31, 334-342.

Manson, S. S., 1966, Thermal Stress and Low-cycle fatigue, McGraw-Hill.

Saiprasertkit, K., Hanji, T., Miki, C., 2012, Fatigue Strength Assessment of Load-carrying Cruciform Joints with Material Mismatching in Low- and High-cycle Fatifue Regions Based on the Effective Notch Concept. International Journal of Fatigue 40, 120-128.

Spiliopoulos, K. V., Panagiotou, K. P., 2012, A Direct Method to Predict Cyclic Steady States of Elastoplastic Structures, Computer Methods in Applied Mechanics and Engineering, 223-224, 186-198.

Srnec Novak, J., De Bona, F., Benasciutti, D., Moro, L., 2018, Acceleration Techniques for the Numerical Simulation of the Cyclic Plasticity Behaviour of Mechanical Components under Thermal Loads, MATEC Web of Conferences, 165, 19010.